Computers and Chemical Engineering 95 (2016) 240–248

Contents lists available at ScienceDirect

Computers and Chemical Engineering

journal homepage: www.elsevier.com/locate/compchemeng

Mathematical modeling and optimal design of multi-stage slug-flow crystallization

Michael L. Rasche, Mo Jiang, Richard D. Braatz*

Department of Chemical Engineering, 77 Massachusetts Avenue, Cambridge, MA 02139, United States

ARTICLE INFO

Article history:
Received 5 September 2016
Accepted 10 September 2016
Available online 28 September 2016

Keywords:
Crystallization
Pharmaceutical engineering
Continuous manufacturing
Particulate processes
Pharmaceutical manufacturing

ABSTRACT

Inspired from experimental progress in continuous crystallizer designs based on air/liquid slug flow that generate crystals of target sizes at high production rates and low capital costs (e.g., Eder et al., 2010; 2011; Jiang et al., 2014; 2015; and citations therein), a mathematical model and procedure are derived for the design of slug-flow crystallizers with spatially varying temperature profiles. The method of moments is applied to a population balance model for the crystals, to track the spatial variation of characteristics of the crystal size distribution along the crystallizer length. Design variables for the cooling slug-flow crystallizer such as tubing lengths and types and numbers of heat exchangers are analyzed and optimized for product crystal quality (e.g., minimized secondary nucleation and impurity incorporation) and experimental equipment costs, while ensuring high yield. This study provides guidance to engineers in the design of slug-flow crystallizers including their associated heat exchanger systems.

1. Introduction

In the pharmaceutical industry, consistent in-spec products from a well-defined robust crystallization process design are crucial for both FDA regulation and operational practice (Yu et al., 2004; Nagy et al., 2008). Continuous-flow tubular crystallizers have shown potential for high reproducibility and process efficiency at low capital and production cost (Alvarez and Myerson, 2010; Lawton et al., 2009; Fergusen et al., 2012; Vacassy et al., 2000; Jiang et al., 2014; Eder et al., 2010, 2011). A technology that combines the advantages of continuous and batch crystallizers is the air/liquid slug-flow crystallizer (Jiang et al., 2014; Eder et al., 2010, 2011, 2012; and citations therein), which has advantages that include narrow residence time distribution, no stirrer for inducing particle attrition/breakage, and easy post-crystallization separation. The potential application of slug-flow crystallization in the final stage of pharmaceutical manufacturing motivates this design study.

As in batch crystallizers (e.g., Nagy and Braatz, 2012; Simon et al., 2015; and citations therein), the robustness of slug-flow crystallization process operation requires an understanding of how the supersaturation profile is affected by design variables (e.g., method and speed of supersaturation generation) and corresponding implementation. For example, supersaturation should be minimized so as to avoid impurity incorporation and secondary nucleation, which is important for slug-flow crystallization due to its typically short residence time (on the order of minutes, Eder et al., 2012; Jiang et al., 2014, 2015) and with fast heat transfer (from the large surface area to volume ratio of tubular crystallizers).

This article presents a design procedure for slug-flow continuous cooling crystallization with the objective of minimizing the maximum supersaturation. Two common methods of cooling are compared: heat baths and double-pipe heat exchangers (Levenspiel, 1962). The effect of design variables on the supersaturation profile is analyzed (e.g., temperatures and locations of heat baths/exchangers, length of tubing). A population balance model for batch crystallization (e.g., Hulburt and Katz, 1964; Randolph and Larson, 1974) is applied to individual slugs, with the batch residence time replaced by continuous residence time (running time). Unlike a past study that mathematical modeled a slug-flow crystallizer (Kubo et al., 1998), this article considers a different crystallization mechanism (cooling crystallization instead of reactive precipitation), different crystallization phenomena (growth of individual crystals instead of aggregation), and not only analyzes our experimental proof-of-concept demonstration (Jiang et al., 2014) but also analyzes the effect of the design variables and applies optimization (e.g., of the number of heat exchangers and the length of tubing in each heat bath/exchanger) while minimizing the total equipment cost.

* Corresponding author.
E-mail address: braatz@mit.edu (R.D. Braatz).

http://dx.doi.org/10.1016/j.compchemeng.2016.09.010
0098-1354/

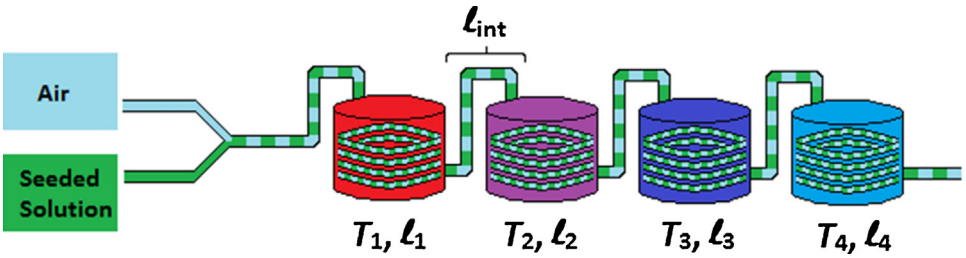

Fig. 1. Schematic for a multiple bath SFC fed with liquid solution with seed crystals, which can be continuously generated by micromixers or an ultrasonic probe (Jiang et al., 2014, 2015). A typical tube is made of silicone of Teflon with an inner diameter of 3.1 mm. During cooling, a typical tank temperature ranges from 60 to 20 ◦ Celsius.

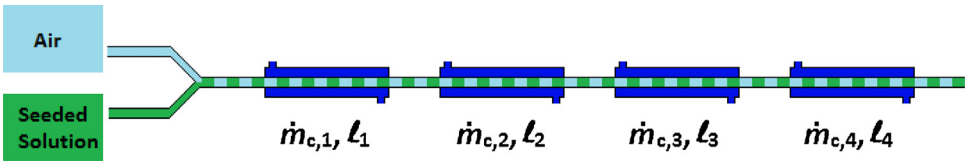

Fig. 2. Schematic for a multiple double-pipe heat exchanger SFC. The temperature of the inlet cooling water in the shell is constant, typically 25 ◦C or lower.

2. Methodology

A well-mixed batch crystallizer can be modeled using the population balance equation (Hulbert and Katz, 1964; Randolph and Larson, 1974)

$$\frac{\partial f}{\partial \tau} + \frac{\partial (Gf)}{\partial L} = B\delta(L - L_0), \tag{1}$$

$$f(\tau = 0, L) = f_0(L), \tag{2}$$

where G and B are growth and nucleation rates, respectively, f is the distribution of particle sizes at residence time τ, L is the particle size, L_0 is the size of nuclei, and δ is the Dirac delta function.

Fig. 1 is a schematic for one of the slug-flow crystallizers investigated in this. For the first system, a liquid solution containing solute and solvent(s) enters a tube and then undergoes ultrasonication under supersaturated conditions to generate seed crystals. The slurry containing seed crystals is then combined with a stream of air under flow conditions in which slugs spontaneously form. The inlet concentration in the slugs is denoted by C_0, and the inlet temperature by T_0. The tube passes first into a bath of temperature T_1. The bath is agitated to provide spatially uniform temperature and to promote heat transfer between the liquid in the bath and outer surface of the tube. The length of tubing inside the first bath is denoted by ℓ_1. The tube then passes into a second bath at a different temperature, T_2. The length of tubing in the second bath is denoted by ℓ_2, and the length of tubing in the interval between (and outside of) adjacent baths in denoted by ℓ_{int}. A total of four temperature baths are included in the experimental configuration.

An alternative system investigated here replaces the constant-temperature baths with counterflow single-pass double-pipe heat exchangers (Fig. 2). While the inlet shell-side temperature is equal for each heat exchanger i, the length ℓ_i and cooling water flowrate $\dot{m}_{c,i}$ can differ (Fig. 3).

3. Mathematical modeling of slugs as batch crystallizers

Experimental evidence indicates that each slug is well-mixed (Kashid et al., 2005; Jiang et al., 2014), so each slug operates as an individual batch crystallizer that is physically transported down the tube. For batch systems under low supersaturation, where nucleation can be considered negligible, the term on the right-hand side of Eq. (1) can be neglected. With the common assumptions of size-independent growth and no growth rate dispersion, the population balance model describing the evolution of the crystal size distribution in each slug is reduced to

$$\frac{\partial f}{\partial \tau} + G\frac{\partial f}{\partial L} = 0 \tag{3}$$

where τ is the time from when a slug enters the first bath. The growth rate can be defined for this system as (Randolph and Larson, 1974)

$$G = k_g[C - C_{sat}(T)]^g \tag{4}$$

where k_g and g are fit to data, C_{sat} is the solubility (aka saturation concentration) as a function of temperature, and C and T are the bulk concentration and temperature, respectively. A typical slug in the first bath starts at the concentration C_0 and temperature T_0 at supersaturated or saturated conditions ($C_0 \geq C_{sat}(T_0)$), inlet seed mass m_{seed}, and inlet crystal size distribution (CSD) f_0.

Attrition, aggregation, agglomeration, breakage, and nucleation within each slug are considered to be negligible, as has been observed in experiments (Jiang et al., 2015). The low levels of these phenomena are associated with the lack of any mixing blade, static mixers, or other internals to induce such phenomena for the

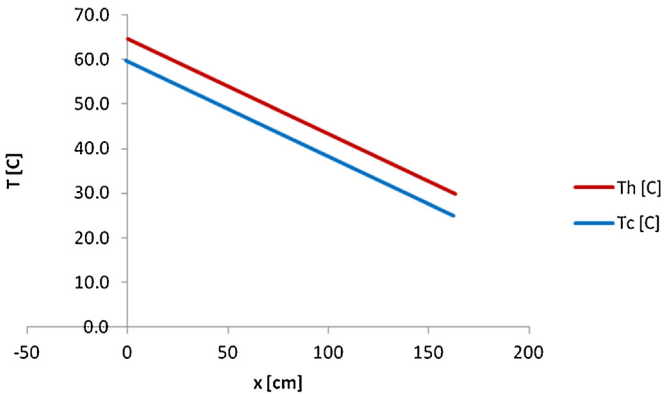

Fig. 3. Estimated temperature profile of a double-pipe heat exchanger designed with constant log mean temperature difference. The red line (upper line) marks the temperature of slugs in the tube and the blue line (lower line) marks the temperature of cooling water in the shell (for interpretation of the references to colour in this figure legend, the reader is referred to the web version of this article).

levels of supersaturation that occur in the experiments. The system of ordinary differential equations

$$\begin{aligned}\frac{d\mu_0}{d\tau} &= 0\\ \frac{d\mu_1}{d\tau} &= G\mu_0\\ \frac{d\mu_2}{d\tau} &= 2G\mu_1\\ &\vdots\end{aligned} \tag{5}$$

is obtained by applying the method of moments (Hulburt and Katz, 1964; Randolph and Larson, 1974) to the population balance model (3), where the kth-order moment μ_k is defined by

$$\mu_k(\tau) = \int_0^\infty f(\tau, L)L^k dL \tag{6}$$

and the inlet conditions are given by the moments calculated from the inlet crystal size distribution f_0.[1] The zeroth-, first-, second-, and third-order moments are proportional to the number, total length, total surface area, and total volume of crystals in a slug. A solute balance for the system is given by

$$\frac{dC}{d\tau} = -3G\rho_c k_v \mu_2 \tag{7}$$

where ρ_c is the crystal density and k_v is the volumetric shape factor. Assuming that the slug is thermally well-mixed and its heat capacity $\hat{C}_p$ is spatially uniform, and that the temperature in the bath is spatially uniform, the total mass and energy balances for a slug are

$$\frac{dm}{d\tau} = 0, \tag{8}$$

$$m\hat{C}_p\frac{dT}{d\tau} = UA(T_i - T) + \frac{m\Delta\tilde{H}_c}{M_c}\frac{dC}{d\tau}, \tag{9}$$

$$T(\tau = 0) = T_0 \tag{10}$$

where m is the mass of a slug, T is the steady-state temperature as a function of residence time τ, U is the overall heat transfer coefficient, A is the surface area for heat transfer, T_i is the temperature of bath i, and $\Delta\tilde{H}_c$ and M_c are the heat of crystallization and molecular weight of the solute molecule respectively.

The analytical solution for the energy balance (Eqs. (9)–(10)) in the first bath is

$$T = T_1 + \exp\left(\frac{-UA\tau}{m\hat{C}_p}\right)\left[\int_0^\tau \exp\left(\frac{UA\tau'}{m\hat{C}_p}\right)\frac{\Delta\tilde{H}_c}{\hat{C}_p M_c}\frac{dC}{d\tau}d\tau' + T_0 - T_1\right]. \tag{11}$$

Similarly for baths 2–4, assuming temperature does not drop at intervals between adjacent baths (the connection tube between baths in well-insulated and the length is minimized), the temperature can be calculated as

$$T = T_i + \exp\left(\frac{-UA(\tau - \tau_i)}{m\hat{C}_p}\right)\left[\int_{\tau_i}^\tau \exp\left(\frac{UA(\tau' - \tau_i)}{m\hat{C}_p}\right)\frac{\Delta\tilde{H}_c}{\hat{C}_p M_c}\frac{dC}{d\tau}d\tau' + T_{i-1} - T_i\right]. \tag{12}$$

The time for which the slug enters bath i,

$$\tau_i = \frac{1}{v}\left[\left(\sum_{j=1}^{i}\ell_{i-1}\right) + \ell_{\text{int}}(i-1)\right], \tag{13}$$

is calculated by assuming a constant velocity v. The overall heat transfer coefficient U is composed of three parts: convective heat transfer within the slug surface, conduction through the tube wall, and convective transfer in the bulk cooling water (bath), that is,

$$\frac{1}{U} = \frac{1}{h_{\text{slug}}} + \frac{d_1 \ln\frac{d_2}{d_1}}{2k_w} + \frac{1}{h_{\text{bath}}}. \tag{14}$$

where d_1 and d_2 are the inside and outside diameters of the tubing, k_w is the thermal conductivity of the tube wall, and h_{slug} and h_{bath} are respective convective heat transfer coefficients. The Sieder-Tate correlation for the Nusselt number (Sieder and Tate, 1936),

$$\text{Nu} = \frac{h_{\text{slug}}d_1}{k_s} = 0.023Re^{0.8}Pr^{1/3}\left(\frac{\mu_{c,s}}{\mu_{w,s}}\right), \tag{15}$$

can be used to determine h_{slug}, where Re and Pr are the Reynolds and Prandtl numbers, respectively, k_s is the thermal conductivity of the slug solution, and the ratio of dynamic viscosities in the last term for the slug solution at the center and wall is assumed to be unity. The value for h_{bath} can be calculated from (Chilton et al., 1944),

$$\text{Nu} = \frac{h_{bath}D}{k_b} = 0.87Re_N^{2/3}Pr^{1/3}\left(\frac{\mu_{c,b}}{\mu_{w,b}}\right)^{0.14}, \tag{16}$$

where D is the inside diameter of the agitated vessel, k_b is the thermal conductivity of the bath fluid (typically water), the last term is the ratio of dynamic viscosities for the bath fluid, and the Reynolds number Re_N for an agitated vessel is given by

$$Re_N = \frac{N\rho_b L_a^2}{\mu_{c,b}}, \tag{17}$$

where N is the agitator speed, L_a is the agitator diameter, and ρ_b and $\mu_{c,b}$ are the density and dynamic viscosity of the bath fluid.

For the multi-bath system, an optimal choice for the bath temperatures and tube lengths is based on the objective of low maximum supersaturation level within the metastable zone, to maintain purity and avoid secondary nucleation within the liquid slugs passing through the tube. In the case of the four-bath system, the optimization is given by

$$\min_{\substack{T_1, T_2, T_3\\ \ell_1, \ell_2, \ell_3, \ell_4}} w_1 \max\left\{0, [C_f - C_{sat}(T_4)]\right\} + w_2 S_{\max} + w_3\sum_i \ell_i \tag{18}$$

where the first term compares the final concentration C_f in the system to $C_{sat}(T_4)$, the saturation concentration at the final temperature, to force high yield. In the second term, $S_{\max}$ is the maximum supersaturation within the system. The third term is the total length of tubing.

The outlet temperatures of a double-pipe heat exchanger can be calculated using the effectiveness defined as (Kays and London, 1984)

$$\eta = \frac{1 - e^{-\alpha}}{1 - \frac{W_c}{W_s}e^{-\alpha}}, \tag{19}$$

for $W_c \neq W_s$, where W_s and W_c are the heat capacity rates of slugs and cooling water ($W = \dot{m}\hat{C}_p$), and the exponent α is defined by

$$\alpha = U\pi d_1 \ell\beta\left(\frac{1}{W_c} - \frac{1}{W_s}\right) \tag{20}$$

where U is the overall heat transfer coefficient, d_1 is the tube diameter and ℓ is the length of the tube. Then the outlet temperature of the slug stream is

$$T_{s,out} = T_{s,in} + \frac{W_c}{W_s}\eta\left(T_{c,in} - T_{s,in}\right) \tag{21}$$

[1] The full crystal size distribution can be constructed from the moments, as discussed in at the end of the Appendix.

where the inlet temperatures $T_{c,in}$ and $T_{s,in}$ of the cooling water and slug stream, respectively, are specified. For $W_c = W_s$, the application of L'Hopital's rule to (25) gives the expression

$$\lim_{W_c \to W_s} \eta = \frac{U\pi d_1 \ell \beta}{U\pi d_1 \ell \beta + W_s}. \tag{22}$$

If curvature caused by the non-constant ΔT_{LM} is neglected, a linear approximation to the temperature in the tube as a function of distance x from the heat exchanger entrance can be derived as (justification given in Supplementary material)

$$T_s(x) = T_{s,in} - \frac{T_{s,out} - T_{s,in}}{\ell} x. \tag{23}$$

For a given inlet temperature of cooling water and total length of tubing, the lengths of tubing in each heat exchanger can be chosen to minimize the supersaturation over the total length of tube while also maximizing the total yield:

$$\begin{aligned} &\min_{\ell_1, \ell_2, \ell_3} \quad \left[S_{\max} + \varepsilon_1 \max\left\{C_f - C_{sat}(T_{c,in}), 0\right\}\right] \\ &\dot{m}_{c,1}, \dot{m}_{c,2}, \dot{m}_{c,3}, \dot{m}_{c,4} \\ &0 < \ell_i \le \ell_{total}, i = 1, \ldots, n \\ &\ell_n = \ell_{total} - \sum_i^{n-1} \ell_i \\ &0 < \dot{m}_{c,i} \le \dot{m}_{c,\max}, i = 1, \ldots, n. \end{aligned} \tag{24}$$

where the value of ε_1 specifies the tradeoff between maximum supersaturation and yield in a system with fixed tube length.

4. Results and discussion

The parameters used in this simulation study are reported in Table 1, with the resulting heat transfer terms in Eq. (14) given in Table 2. The analytical expression for the solubility as a function of temperature used in this article is taken from Jiang et al. (2012):

$$C_{sat} = 3.084 \times 10^{-2} - 1.373 \times 10^{-3} T + 5.214 \times 10^{-5} T^2. \tag{25}$$

4.1. Constant-temperature baths

For the multi-bath system described above, the optimal design parameters determined by numerical solution of Eq. (18) for literature values of the growth kinetics are reported in the first row of Table 3, with the associated simulation outputs shown in Fig. 4. Table 3 also reports optimal design parameters corresponding to 20% relative error in the growth kinetic parameters, with the associated simulation results in Fig. 4 as well.

All of the optimal designs in Fig. 4 have four peaks of supersaturation with roughly equal height, as determined by the bath temperature, except for the case of increased g, in which the corresponding decrease in growth rate is so high that only the first peak occurs for the fixed residence time. The optimal lengths allow the supersaturation to approach zero before entering a new bath. Increasing g or decreasing k_g slows the growth kinetics and so increases the length of tubing (and residence time) needed to achieve the desired yield (Table 3). The value of the growth exponent g has a large effect on the growth kinetics, and correspondingly, the length of tubing required. Variation in the growth kinetics has a comparatively small effect on the values of the optimal bath temperatures and the maximum supersaturation.

Alternatively, Table 4 shows the effect of 20% error in the growth kinetic parameters if not taken into account in the design calculations. To construct this table, the length and temperature values given by the first row of Table 3 are used in the SFC design, but the values of the growth kinetic parameters are altered as shown to demonstrate the robustness of the nominal process design to uncertainties in the growth kinetics. Fig. 5 shows the simulation results corresponding to the rows of Table 3.

When the true growth kinetics are faster than assumed in the process design calculations, the lengths corresponding to the original growth rate are more than sufficient, so a slight improvement is seen in the yield, and the maximum supersaturation remains unaffected (Table 4). When the true growth rate is 20% slower (last row in Table 4), there is a modest decrease in yield and increase in the maximum supersaturation. When the true growth kinetics are much slower than used in the design calculations (g + 20%), the yield is much lower and the peak supersaturation is much higher, which would result in lower molecular purity of the product crystals. If

Table 1
Model parameters used in the simulation study. The crystallization kinetic parameters in rows 1 and 2 are for L-asparagine monohydrate (LAM) in aqueous solution from Jiang et al. (2012), the crystallizer equipment parameters are for the experimental slug-flow crystallizer implemented by Jiang et al. (2014), and the thermal conductivity is for silicone rubber (Incropera and DeWitt, 2002). The values of the weights w_1 to w_3 were selected using an iterative approach, where the optimal parameters for given weights were input to the simulation and results were visually inspected.

Variable	Value	Units
k_g	6.353	(μm-g solution)/(s-g LAM)
g	1.0	unitless
β	0.25	unitless
$\Delta\tilde{H}_c$	−35700	J/mol
$\mu_{b,c}$	0.001	Pa-s
$\mu_{b,w}$	0.001	Pa-s
$\mu_{s,c}/\mu_{s,w}$	1	unitless
ρ_b	1000	kg/m^3
ρ_c	1543	kg/m^3
A[a]	$\pi(0.0031)(0.003)$	m^3
C_0	0.16	g LAM/g solution
$\hat{C}^b_{p,c}$	4187	J/(kg-K)
$\hat{C}^b_{p,h}$	4187	J/(kg-K)
d_1	0.0031	m
d_2	0.006	m
D	0.15	m
k_b	0.597	W/(m-K)
k_s	0.597	W/(m-K)
k_v	1.0	dimensionless
k_w	0.14	W/(m-K)
L_a	0.06	m
m_{seed}	2.86×10^{-9}	g
$m_{solvent}$	2.12×10^{-2}	g
$\dot{m}^c_h$	4.24×10^{-2}	g/s
M_c	0.150	kg/mol
N	1	1/s
T_0	64.6	°C
$T_{c,in}$	20.0	°C
w_1	5×10^3	g solution/g LAM
w_2	5×10^3	g solution/g LAM
w_3	0.1	1/m

[a] The slug-wall contact area A assumes a slug with contact that is 3 mm long with a tube that has inner diameter of 3.1 mm. The slug length is selected to be about equal to the inner diameter so as to maximize the mixing in each slug, as shown in images of Jiang et al. (2014).
[b] The heat capacities of the cold and hot streams are approximated as the heat capacity of water.
[c] The slug mass of 2.12×10^{-2} g multiplied by the slug flowrate of 2 slugs per second.

Table 2
Comparison of contributions to the overall heat transfer coefficient[a] for a four-tank SFC case study with model parameters taken from experiments. The tube wall provides the largest resistance to heat transfer.

h_{slug}	h^b_{wall}	h_{bath}	U
327	137	1560	96.4

[a] numerical values given in SI units: $\frac{\mathrm{W}}{\mathrm{m^2K}}$.
[b] thermal conductance of the wall: $h_{wall} = 2k_w \left(d_1 \ln \frac{d_2}{d_1}\right)^{-1}$.

Table 3
Optimal parameters for the four-tank SFC calculated for approximate maximum and minimum values of growth kinetic parameters[a].

	T_1	T_2	T_3	ℓ_1	ℓ_2	ℓ_3	ℓ_4	ℓ_{tot}	S_{max}	C_f
Literature[b]	59.1	52.5	43.5	71.8	34.4	21.5	23.2	151	0.0279	0.0372
$g+20\%$	58.6	51.5	42.5	169	70.4	34.1	77.4	351	0.0305	0.0370
$k_g+20\%$	59.4	52.5	43.6	78.1	31.5	22.2	27.1	159	0.0268	0.0367
$k_g-20\%$	58.9	52.1	43.0	81.3	37.0	20.5	29.3	166	0.0293	0.0371

[a] Parameter values are shown in °C for temperature, m for length, and g/g solvent for concentration.
[b] $g \approx 1.0$ (Jiang et al., 2012), so $g-20\%$ is infeasible for this case study.

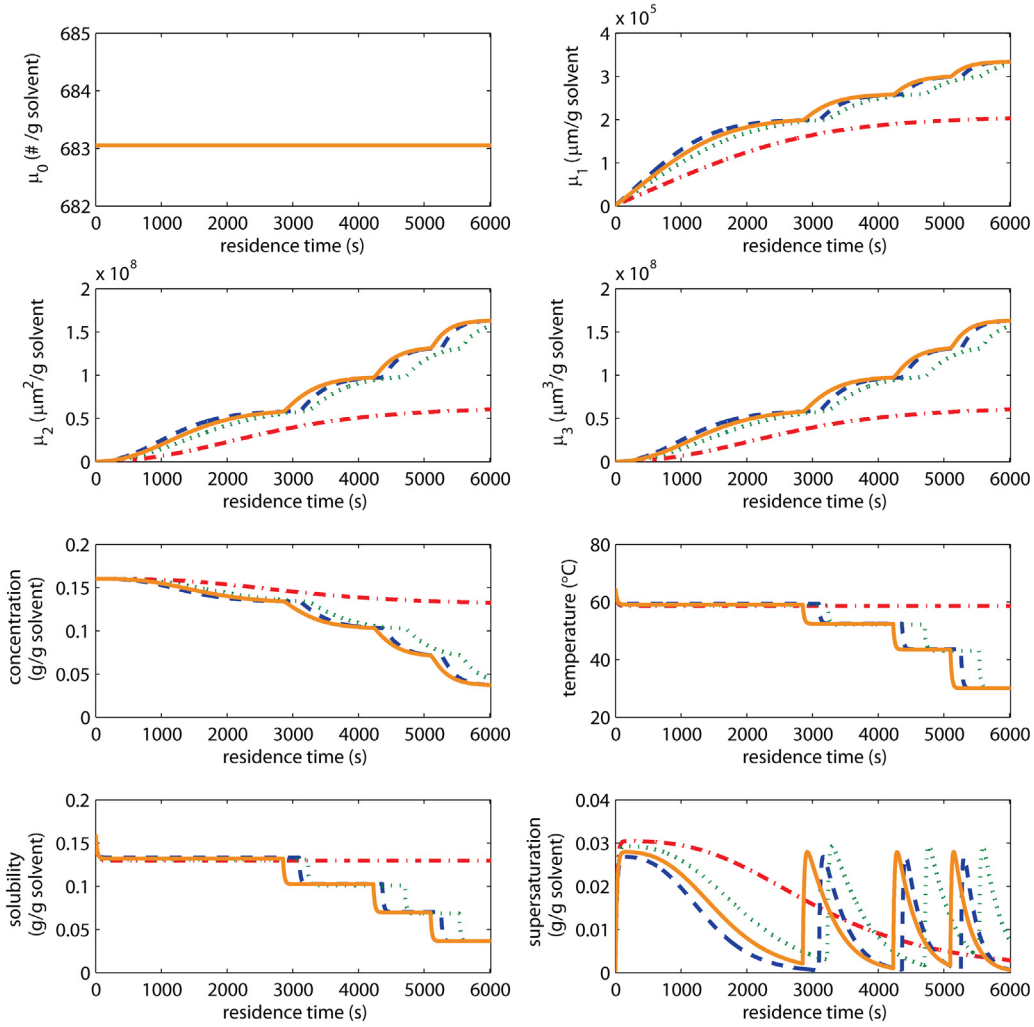

Fig. 4. Simulation results for the optimal parameters calculated using literature values of the growth kinetics parameters (−) and with 20% relative error in the literature values: $1.2g$ (−·), $1.2k_g$ (−−), $0.8k_g$ (···). The residence time shown is the literature value. The effects of varying k_g is rather modest, whereas the 20% increase in the growth exponent g significantly lowers the growth rate, so that the yield is very low over the fixed residence time.

Table 4
Effect of using optimum calculated from literature values of growth parameters when the true system values are off by 20%[a].

	S_{max}	C_f
Literature[b]	0.0279	0.0372
$g+20\%$	0.0446	0.0449
$k_g+20\%$	0.0279	0.0368
$k_g-20\%$	0.0316	0.0380

[a] The units for solute concentration are g/g solvent.
[b] $g \approx 1.0$ (Jiang et al., 2012), so $g-20\%$ is infeasible for this case study.

the increase in maximum supersaturation is not overly detrimental to molecular purity, a precautionary increase in the final tube length as a safety margin would still guarantee that the maximum yield is attained for the given final temperature.

The peak supersaturation obtained in each tank is approximately the same as the other three tanks for the full range of uncertainties in the growth kinetics (Fig. 5). For all cases in Figs. 4–5, the slug temperature at the inlet of each tank initially drops quickly and is then relatively constant to the exit. Also in all cases, the spatial profiles for the solute concentration are flat near the inlet of the first tank, which is because the low initial total surface area of seed crystals in each slug limits the mass deposition rate on the crystals. The solute concentration continues to drop slowly but more quickly as the total surface area of crystals increases as each slug moves down the tube.

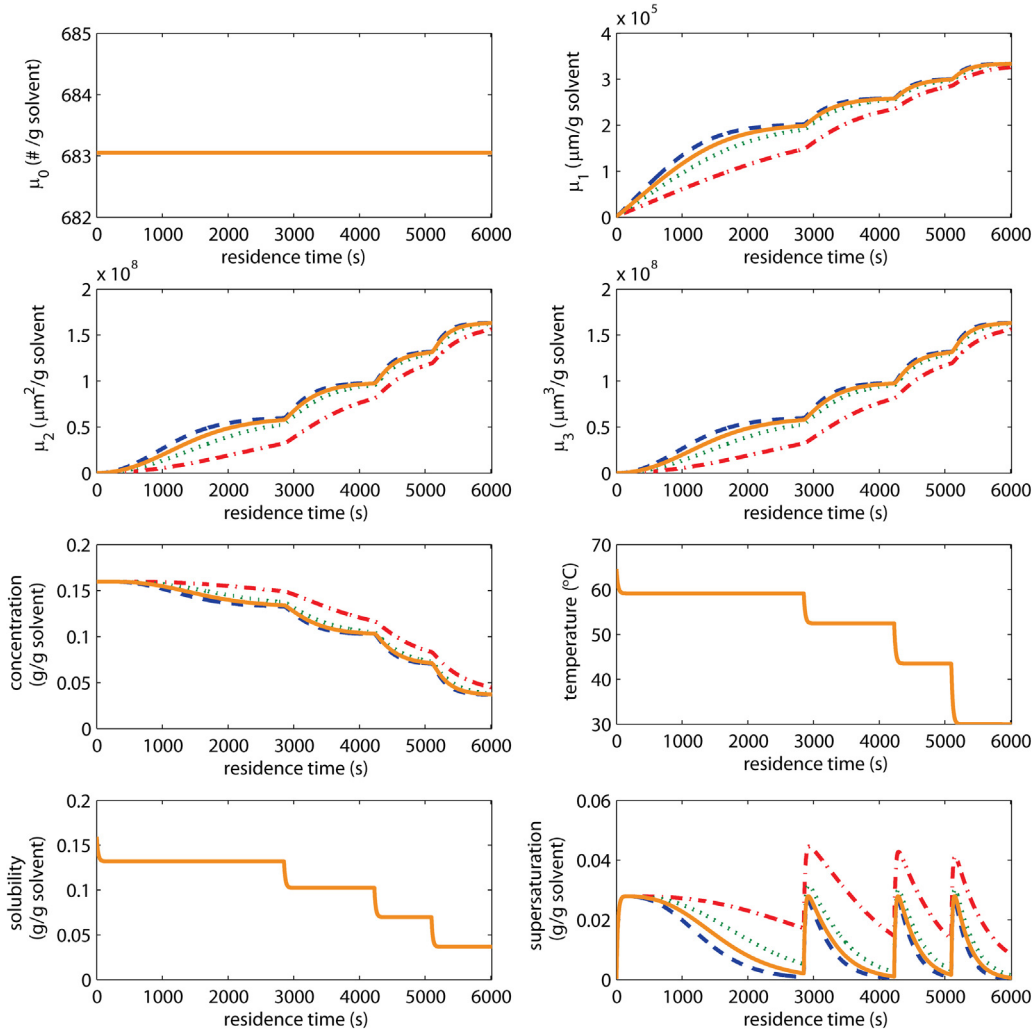

Fig. 5. Simulation results showing the effects of uncertainty in the growth kinetics parameters using the optimal operating conditions predicted by literature values (−) but then introducing a 20% error in the parameters: $1.2g$ (−·), $1.2k_g$ (−−), $0.8k_g$ (···). A decreased growth rate results in higher supersaturation peaks and lower yield, while an increased growth rate increases yield.

4.2. Double-pipe heat exchangers

For double-pipe heat exchangers in series, for each heat exchanger, the optimum occurs when the length of the tube approaches infinity, and the cooling water flowrate is high enough to remove all of the excess heat from the system (Fig. 6). These conditions cause the peak supersaturation to approach zero while the yield approaches its maximum value. In a practical system, the total tube length are cooling water flowrates are finite. If the cooling water flowrate is given a maximum value of 50 mg/s and the total length of tubing is restricted to 300 m, the Pareto-optimality curve in Fig. 7 can be constructed from the data in Table 5 for n heat exchangers in series. Fig. 7 demonstrates the tradeoff between the two objectives as well as the diminishing returns of adding more heat exchangers beyond $n = 3$. The simulation results around the tradeoff point (the leftmost non-trivial solution) are shown in Fig. 8 for each value of n.

Fig. 8 shows an increase in the number of supersaturation peaks as the number of heat exchangers increase, with the values of supersaturation in this system lower than predicted by the multi-bath system by a factor of three, due to the improved spatial temperature profiles obtained by counterflow heat exchange. The solute concentration near the inlet of the first tank is very flat for a significant slug residence time in the tube, and the smoother

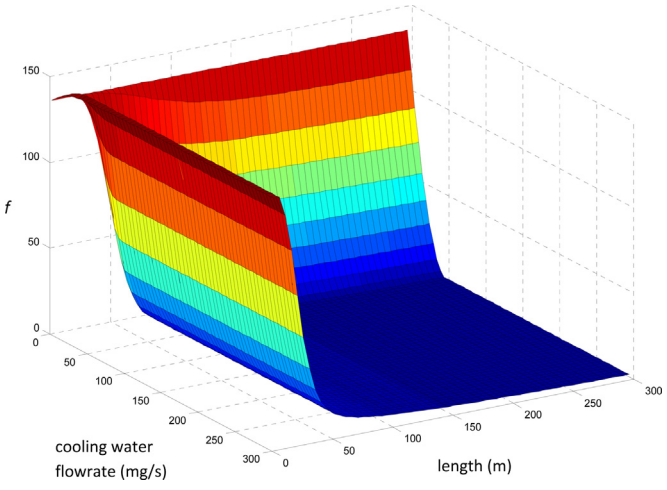

Fig. 6. The objective function for the double-pipe SFC (Eq. (24)) is plotted for a single heat exchanger ($n = 1$), when total length and cooling water flowrate take on a large range of values.

reduction in temperature results in a smoother reduction in solubility, and a smoother increase in the supersaturation. Once the

Table 5
Optimal parameters for the double-pipe SFC for different values of ε_1 in Eq. (24) and different numbers of heat exchangers, n. The range of values (in meters) for the lengths is [0,300] and the range for the cooling water flowrate (in mg/s) is [0.001,50]. The below data are used to construct the Pareto-optimality curve (Fig. 7).

n	ε_1	ℓ_1	ℓ_2	ℓ_3	ℓ_4	$\dot{m}_{c,1}$	$\dot{m}_{c,2}$	$\dot{m}_{c,3}$	$\dot{m}_{c,4}$
1	0.01	300				0.001			
	0.1	300				0.001			
	0.18	300				0.001			
	0.19	300				34			
	0.2	300				35			
	0.25	300				40			
	0.5	300				50			
	1	300				50			
2	0.01	170	130			0.001	0.001		
	0.1	156	144			6	43		
	1	146	154			6	50		
	10	110	190			5	49		
	100	273	27			50	27		
3	0.01	300	0	0		0.001	0.001	0.001	
	0.1	153	96	51		4.3	17	49	
	0.5	161	130	9		6.9	49	1.4	
	1	154	136	10		6.6	50	3.9	
	10	144	134	22		7	50	48	
	100	273	12	15		50	48	46	
4	0.001	300	0	0	0	0.001	0.001	0.001	0.001
	0.01	119	53.4	62.4	65.2	2.91	4.28	13.3	50
	0.1	119	58.4	57.6	65.0	2.91	4.71	13.2	50
	1	139	73	75	13	12	49	15	50
	10	138	75	62	25	4	14	50	49

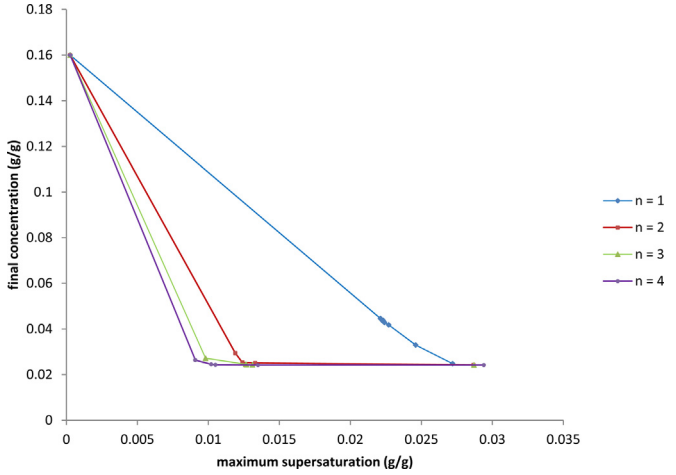

Fig. 7. Pareto-optimality curves for the double-pipe SFC with different total number of heat exchangers at a constant total tube length of 300 m, with data reported in Table 5. Each point on a Pareto-optimality curve is optimal for a partial weighting of the two competing objectives. Given the economic incentive is high to maintain high yield, the most practical optimum would be near the "knee" of each curve.

supersaturation reaches its peak, it does not drop as low for the double-pipe heat exchangers as for the constant-temperature baths (cf Figs. 4–5 with Fig. 8)—the maintenance of a persistent significantly positive supersaturation enables the peak supersaturation to be lower for the double-pipe exchangers while achieving the same yield as the constant-temperature baths. Note that the yield in any system of heat exchangers is theoretically restricted by the minimum system temperature given that a sufficient length of tubing is available, so installing extra tubing is a way to ensure that the desired yield is obtained. The larger the uncertainty in the growth kinetics, the larger the extra tubing should be.

5. Conclusions

Mathematical models and design procedures are proposed for two continuous slug-flow crystallization systems. By combining constant-temperature cooling baths in series, the temperature of the slugs is stepped down gradually to maintain low supersaturation, to promote growth over nucleation, while allowing high yield. The advantage of simplicity is offset by relatively high spikes in supersaturation at the inlet to each bath. An alternative system is investigated that uses multiple counterflow double-pipe heat exchangers in series to reduce the temperature more gradually. The double-pipe heat exchange system provides similar high yield, while reducing the maximum supersaturation by a factor of three in a case study using realistic experimental values for the parameters. In the case study, it was observed that increasing the number of heat exchangers beyond three had only a small effect on the optimal design objective and tradeoff curve (Fig. 7). For either heat exchanger design, an extra length of tubing can be used to ensure that the desired yield is achieved for a specified uncertainty in growth kinetics (Fig. 6).

Acknowledgement

Novartis is acknowledged for support of this work.

Appendix A.

The inlet initial crystal size distribution in the simulation study is given by a quadratic function (e.g., Chung et al., 2000; Togkalidou et al., 2004)

$$f_0(L) = \begin{cases} aL^2 + bL + c, & \text{for} L_{\min} \le L \le L_{\max} \\ 0, & \text{otherwise} \end{cases} \tag{A1}$$

The CSD is assumed symmetrical with the peak at $\bar{L} = 5$ μmand distribution width $w = 2$ μm, which are estimated based on optical microscopy measurement. Eq. (A1) is equal to zero at $L = \bar{L} \pm w/2$, so that

$$L_{\min} = \bar{L} - \frac{w}{2}, \tag{A2}$$

$$L_{\max} = \bar{L} + \frac{w}{2}. \tag{A3}$$

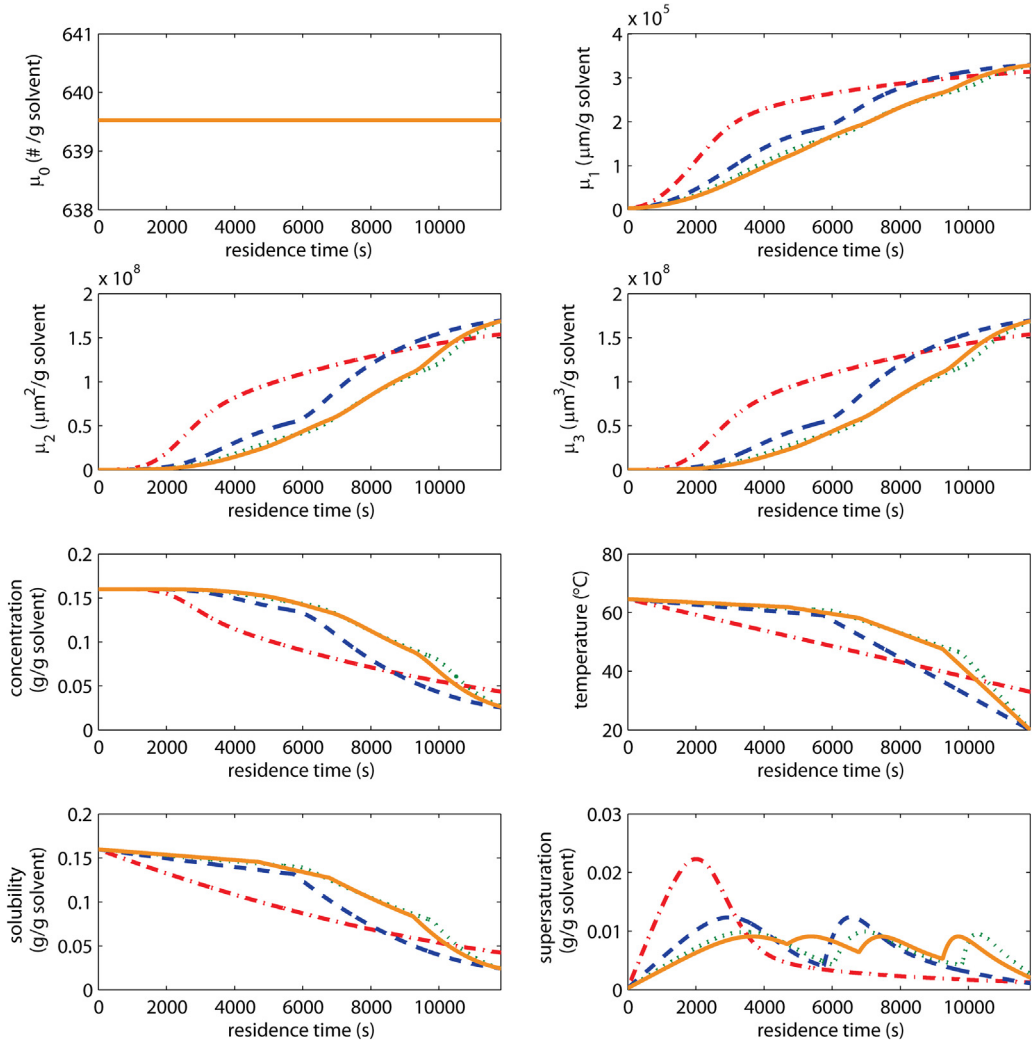

Fig. 8. Simulation results for the double-pipe SFC near the tradeoff point for $n = 1(-\cdot)$,$n = 2\,(--)$,$n = 3(\cdots)$, and $n = 4(-)$. Using two heat exchangers instead of one decreases the maximum supersaturation by about a factor of two. Additional heat exchangers offer an ever-diminishing return on investment.

The parameters a, b, and c in Eq. (A1) can be determined by analytically solving the system of linear equations

$$(L_{\max}^6 - L_{\min}^6)\frac{a}{6} + (L_{\max}^5 - L_{\min}^5)\frac{b}{5} + (L_{\max}^4 - L_{\min}^4)\frac{c}{4} = \frac{m_{seed}}{m_{solvent}\rho_c}, \tag{A4}$$

$$aL_{\max}^2 + bL_{\max} + c = 0, \tag{A5}$$

$$aL_{\min}^2 + bL_{\min} + c = 0. \tag{A6}$$

where the first equation is obtained by integrating L^3 multiplied by (A1) to determine the crystal mass per mass solvent, and the volume shape factor is assumed to be equal to one.

While this article uses moments to describe the evolution of the size distribution, the system (3)–(4) with initial condition (A1) is an example of the 1D advection equation with solution given by

$$f(\tau, L) = f_0\left(L - \int_0^\tau G d\tau'\right), \tag{A7}$$

that is, the solution to the PBE is a translation of the initial distribution. Recognizing that the integral in (A7) can be calculated by integrating the second differential equation of (5),

$$\int_0^\tau G d\tau' = \frac{\mu_1(\tau) - \mu_1(0)}{\mu_0}, \tag{A8}$$

the crystal size distribution can be constructed.

Appendix B. Supplementary data

Supplementary data associated with this article can be found, in the online version, at http://dx.doi.org/10.1016/j.compchemeng.2016.09.010.

References

Alvarez, A.J., Myerson, A.S., 2010. Continuous plug flow crystallization of pharmaceutical compounds. Cryst. Growth Des. 56, 349–369.
Chilton, T.H., Drew, T.B., Jenkins, R.H., 1944. Heat transfer coefficients in agitated vessels. Ind. Eng. Chem. 36 (6), 510–516.
Chung, S.H., Ma, D.L., Braatz, R.D., 2000. Optimal experimental design in batch crystallization. Chemom. Intell. Lab. Syst. 50, 83–90.
Eder, R.J.P., Radl, S., Schmitt, E., Innerhofer, S., Maier, M., Gruber-Woelfler, H., Khinast, J.G., 2010. Continuously seeded continuously operated tubular crystallizer for the production of active pharmaceutical ingredients. Cryst. Growth Des. 10 (5), 2247–2257.
Eder, R.J.P., Schmitt, E.K., Grill, J., Radl, S., Gruber-Woelfler, H., Khinast, J.G., 2011. Seed loading effects on the mean crystal size of acetylsalicylic acid in a continuous-flow crystallization device. Cryst. Res. Technol. 46 (3), 227–237.
Eder, R.J.P., Schrank, S., Besenhard, O., Roblegg, E., Gruber-Woelfler, H., Khinast, J.G., 2012. Continuous sonocrystallization of acetylsalicylic acid (ASA): control of crystal size. Cryst. Growth Des. 12 (10), 4733–4738.
Ferguson, S., Morris, G., Hao, H., Barrett, M., Glennon, B., 2012. In-situ monitoring and characterization of plug flow crystallizers. 18th International Symposium on Industrial Crystallization 77, 105–111.
Hulburt, H.M., Katz, S., 1964. Some problems in particle technology. A statistical mechanical formulation. Chem. Eng. Sci. 19 (8), 555–574.

Incropera, F.P., DeWitt, D.P., 2002. Fundamentals of Heat and Mass Transfer, 5th ed. Wiley, Hoboken, NJ.
Jiang, M., Wong, M.H., Zhu, Z., Zhang, J., Zhou, L., Wang, K., Ford Versypt, A.N., Si, T., Hasenberg, L.M., Li, Y.E., Braatz, R.D., 2012. Towards achieving a flattop crystal size distribution by continuous seeding and controlled growth. Chem. Eng. Sci. 77, 2–9.
Jiang, M., Zhu, Z., Jimenez, E., Papageorgiou, C.D., Waetzig, J., Hardy, A., Langston, M., Braatz, R.D., 2014. Continuous-flow tubular crystallization in slugs spontaneously induced by hydrodynamics. Cryst. Growth Des. 14 (2), 851–860.
Jiang, M., Papageorgiou, C.D., Waetzig, J., Hardy, A., Langston, M., Braatz, R.D., 2015. Indirect ultrasonication in continuous slug-flow crystallization. Cryst. Growth Des. 15 (5), 2486–2492.
Kashid, M.N., Gerlach, L., Goetz, S., Franzke, J., Acker, J.F., Platte, F., Agar, D.W., Turek, S., 2005. Internal circulation within the liquid slugs of a liquid–liquid slug flow capillary microreactor. Ind. Eng. Chem. Res. 44 (14), 5003–5010.
Kays, W.M., London, A.L., 1984. Compact Heat Exchangers, 3rd ed. McGraw-Hill, New York.
Kubo, M., Kawakatsu, T., Yonemoto, T., 1998. Modelling of continuous synthesis process of TiO_2 particles using slug-flow tubular reactor. Chem. Eng. Res. Des. 76 (6), 669–676.
Lawton, S., Steele, G., Shering, P., Zhao, L., Laird, I., Ni, X.-Y., 2009. Continuous crystallization of pharmaceuticals using a continuous oscillatory baffled crystallizer. Org. Process Res. Dev. 13 (6), 1357–1363.
Levenspiel, O., 1962. Chemical Reaction Engineering: An Introduction to the Design of Chemical Reactors. Wiley, New York.
Nagy, Z.K., Braatz, R.D., 2012. Advances and new directions in crystallization control. Annu. Rev. Chem. Biomol. Eng. 3, 55–75.
Nagy, Z.K., Fujiwara, M., Braatz, R.D., 2008. Modeling and control of combined cooling and antisolvent crystallization processes. J. Process Control 18, 856–864.
Randolph, A.D., Larson, M.A., 1974. Theory of Particulate Processes: Analysis and Techniques of Continuous Crystallization, volume 2nd. Academic Press, New York.
Sieder, E.N., Tate, G.E., 1936. Heat transfer and pressure drop of liquid in tubes. Ind. Eng. Chem. 28 (12), 1429–1435.
Simon, L.L., Pataki, H., Marosi, G., Meemken, F., Hungerbühler, K., Baiker, A., Tummala, S., Glennon, B., Kuentz, M., Steele, G., Kramer, H.J.M., Rydzak, J.W., Chen, Z., Morris, J., Kjell, F., Singh, R., Gani, R., Gernaey, K.V., Louhi-Kultanen, M., O'Reilly, J., Sandler, N., Antikainen, O., Yliruusi, J., Frohberg, P., Ulrich, J., Braatz, R.D., Leyssens, T., von Stosch, M., Oliveira, R., Tan, R.B.H., Wu, H., Khan, M., O'Grady, D., Pandey, A., Westra, R., Delle-Case, E., Pape, D., Angelosante, D., Maret, Y., Steiger, O., Lenner, M., Abbou-Oucherif, K., Nagy, Z.K., Litster, J.D., Kamaraju, V.K., Chiu, M.-S., 2015. Assessment of recent process analytical technology (PAT) trends: a multiauthor review. Org. Process Res. Dev. 19, 3–62.
Togkalidou, T., Tung, H.-H., Sun, Y., Andrews, A., Braatz, R.D., 2004. Parameter estimation and optimization of a loosely-bound aggregating pharmaceutical crystallization using in-situ infrared and laser backscattering measurements. Ind. Eng. Chem. Res. 43, 6168–6181.
Vacassy, R., Lemaitre, J., Hofmann, H., Gerlings, J.H., 2000. Calcium carbonate precipitation using new segmented flow tubular reactor. AIChE J. 46 (6), 1241–1252.
Yu, L.X., Lionberger, R.A., Raw, A.S., D'Costa, R., Wu, H., Hussain, A.S., 2004. Applications of process analytical technology to crystallization processes. Adv. Drug Deliv. Rev. 56, 349–369.